sustainability

MDPI

Article

Energy-Based Evaluation on Soil–Structure-Interaction-Related Damping of Inelastic Bridge Pier Structure Subjected to Pulse-like Velocity Ground Motion

Kuo-Hung Chao [1], Yu-Chi Sung [1,*], Xiao-Qin Liu [2] and Chin-Kuo Su [2]

[1] Department of Civil Engineering, National Taipei University of Technology, Taipei 10608, Taiwan
[2] Research Center of Offshore Wind Power Engineering, National Taipei University of Technology, Taipei 10608, Taiwan
* Correspondence: sungyc@ntut.edu.tw; Tel.: +88-622-7712-171

Abstract: This study proposed a procedure of using the energy method to evaluate the SSI-related damping effect when the soil–structure interaction (SSI) was considered in a bridge pier system, which can thus be deemed a soil–foundation–superstructure (SFS) inelastic system. Firstly, the SSI is implemented by adopting a discrete-time recursive filter approach as well as frequency-dependent foundation–soil impedance functions to solve for the external soil forces exerted onto the foundation. Then, by integrating such external soil forces into the motion equations of the SSI-based SFS system, the energy equations can be formulated during the ground motions. To demonstrate the proposed procedure, an implementation study involving a bridge pier was carried out, considering two earthquake recordings. The resultant energy quantities and SSI-related damping ratio shed light on how the aspects of earthquake characteristics affected the energy dissipation mechanism of the bridge pier SSI-based SFS system. This proposed procedure renders a promising solution for quantifying the soil role in the seismic energy dissipation of arbitrary single- and multiple-degree-of-freedom systems considering the SSI effect. The results obtained show that the SSI effect was suppressed when the SFS system underwent near-fault earthquakes, which illustrated that the stiffness and damping contribution from the soil was not pronounced. Furthermore, near-fault earthquakes with large incremental velocities may lead to a low SSI-related damping ratio (SSIDR).

Keywords: discrete-time infinite impulse response filter (IIRF); soil–foundation–superstructure (SFS) system; structural inelasticity; energy quantity; SSI-related damping ratio (SSIDR)

Citation: Chao, K.-H.; Sung, Y.-C.; Liu, X.-Q.; Su, C.-K. Energy-Based Evaluation on Soil–Structure-Interaction-Related Damping of Inelastic Bridge Pier Structure Subjected to Pulse-like Velocity Ground Motion. *Sustainability* **2023**, *15*, 7401. https://doi.org/10.3390/su15097401

Academic Editors: Yi Bao, Yazhou (Tim) Xie, Shan Li and Wenwei Wang

Received: 6 March 2023
Revised: 19 April 2023
Accepted: 26 April 2023
Published: 29 April 2023

1. Introduction

The soil–structure interaction (SSI) is crucial in evaluating structural responses. When sitting on a flexible soil bed, a system considering the SSI effect exhibits a larger structural period than the system without SSI consideration. Many studies have investigated the SSI effects on the dynamic performance of structures [1–6] and on the structural ductility and strength demand [7–13].

The stiffness and dynamic characteristics of soil are highly sensitive to the properties of soil contents and superstructure characteristics. To account for these characteristics, Gazetas [14] proposed a complex frequency-dependent foundation–soil impedance (FSI) function consisting of both real and imaginary components. The real component indicates the stiffness and inertia of the supporting soil, whereas the imaginary component reflects the radiation and material damping of the foundation–soil impedance system. Since Gazetas' work, numerous studies have been conducted to address various soil modeling issues, such as the incorporation of embedded, non-circular, non-rigid, or piled foundations [15–17].

The frequency-dependent nature of soil often necessitates frequency-domain analyses when formulating the equation of motion for the SFS system. However, this approach can come at the cost of losing the benefits that time-domain analysis offers. Incorporating

SSI into standard time-history analysis can be achieved by using a method proposed by Safak [18], which involves approximating the frequency-dependent FSI function in the time domain using a discrete-time digital filter. This allows for the definition of the relationship between foundation forces and displacements through resultant time-domain finite-difference equations. Gash et al. [19] later applied this method to solve the multiple-degree-of-freedom (MDOF) motion equation of a shear building supported by a rigid disk foundation and uniform-soil half-space. Another approach was taken by Sung et al. [20], who used a z-transformed discrete-time infinite impulse response filter as a foundation–soil impedance function. They derived a transfer function between ground displacement and foundation shear, which allowed for the analysis of structural responses using the base force propagating function.

The structural damping mechanism typically results in the dissipation of energy, which can be quantified by the viscous damping ratio. This ratio takes into account all sources of energy dissipation and condenses them into a few basic modal parameters. This approach streamlines the motion equations and provides trustworthy outcomes, making it widely employed in both academic research and practical design applications. To determine radiation damping, the ATC3-06 [21] and ASCE [22] standards utilize Veletsos' technique [23] for assessing the structural and soil parameters. These standards propose that when evaluating foundation damping, it is important to account for both the radiation damping and soil material damping's energy dissipation effects.

Among these two damping items, the radiation damping is dependent on the geometry of the foundation–soil contact area, the structural properties, and the soil properties. The soil material damping can be calculated from the stress–strain response in a steady-state cyclic loading using a variety of testing techniques. However, this method is only accurate as the system is in resonance [24]. In addition, due to the frequency-dependent properties of soil, the soil material damping and radiation damping cannot be directly added into the seismic numerical analysis.

Time integration and motion equation are often used for solving the energy equation of motion. By constructing and solving the energy motion equation, McKevitt et al. [25] evaluated the input energy, hysteretic energy, and the ratio of the cumulative hysteretic energy to the input energy for both single-degree-of-freedom (SDOF) and MDOF systems subjected to four earthquake records. They concluded that the input energy dissipated by the hysteretic mechanism was approximately the same for all four earthquake records.

Uang et al. [26] proposed two procedures for computing the earthquake input energy: one procedure was based on the absolute motion, whereas the other was based on the relative motion. Bruneau et al. [27] believed that the input energy derived from the relative motion method was more sensible than that from the absolute motion method. Hu et al. [28] calculated the additional equivalent damping ratio of an external damping device through energy equations. That is, the ratio of the energy consumption of inherent damping to that of the added dampers can be obtained under external excitations in the time-history analysis. Unlike the strain energy method, this method can eliminate the effect of the excitation frequency on the additional equivalent damping ratio.

From the literature reviewed above, many studies have investigated SSI's effects, inelastic structural behaviors, near-fault earthquakes, and energy dissipation considering SSI-related damping sources. However, few papers have been concerned with the following aspects together: (1) the implementation of the SSI effect through a frequency-dependent FSI function; (2) the energy quantities of yielding energy due to structural inelasticity and SSI-related energy; and (3) near-fault ground motions, which induce different structural responses to far-field earthquakes.

In view of this, this study aimed to develop a procedure for evaluating the SSI-related damping effect, through an energy perspective, on the responses of bridge pier structures. This evaluation procedure first constructs a soil–foundation–superstructure (SFS) system by expanding an inelastic SDOF system to include a frequency-dependent SSI model via the discrete-time infinite impulse response filter (IIRF) technique. Then, based on the motion

equations of the SSI-based SFS system, the energy equations were formulated to distinguish distinct energy quantities in a quantitative manner, particularly the SSI-related energy. The SSI-related damping ratio (SSIDR) was also introduced herein. An implementation study was conducted not only to demonstrate the proposed evaluation procedure, but also to compare the response variance between distinct input earthquake recordings.

This paper proceeds as follows. In Section 2, the methodology of the evaluation procedure is developed. The implementation study is in Section 3. Conclusions are addressed in the last section.

2. Methodology

2.1. Soil–Foundation–Superstructure System

Figure 1a shows an SDOF system sitting on fixed base. The SSI effect is not considered by assuming the fixed-base SDOF system subject to the free-field ground motion. To consider the SSI effect, a 3DOF SSI-based SFS system was constructed by expanding the SDOF system, comprising the underlying soil, foundation, and superstructure, as shown in Figure 1b. The SFS system includes a set of 3DOF, which encompasses the horizontal displacement u_s of the superstructure mass, the horizontal displacement u_{FIM}, and the rotational angle θ_f at the foundation level.

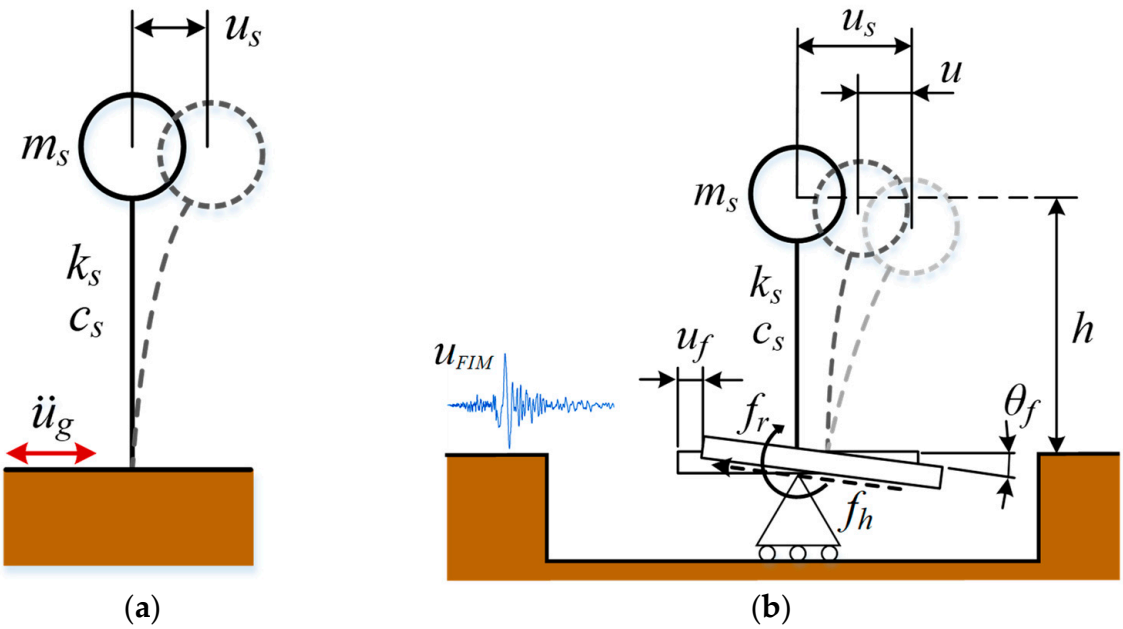

Figure 1. Structural models: (**a**) the fixed-base SDOF system and (**b**) the SSI-based SFS system.

In Figure 1b, m_s, c_s, and k_s denote the mass, damping, and stiffness of the superstructure, respectively, u_s is the mass-to-ground relative displacement, and u_f is the foundation-to-ground relative displacement. The collective soil–foundation dynamic stiffness and damping properties are approximated as the transitional and rotational forces—f_h and f_r—at the foundation level. Figure 2 illustrates the process flowchart for determining the transitional and rotational forces using the IIRF technique.

In this context, the method proposed by Veletsos et al. [16], Sieffert et al. [24], and Safak [18] was utilized to calculate the transitional and rotational forces, which are not explicitly discussed for the sake of brevity.

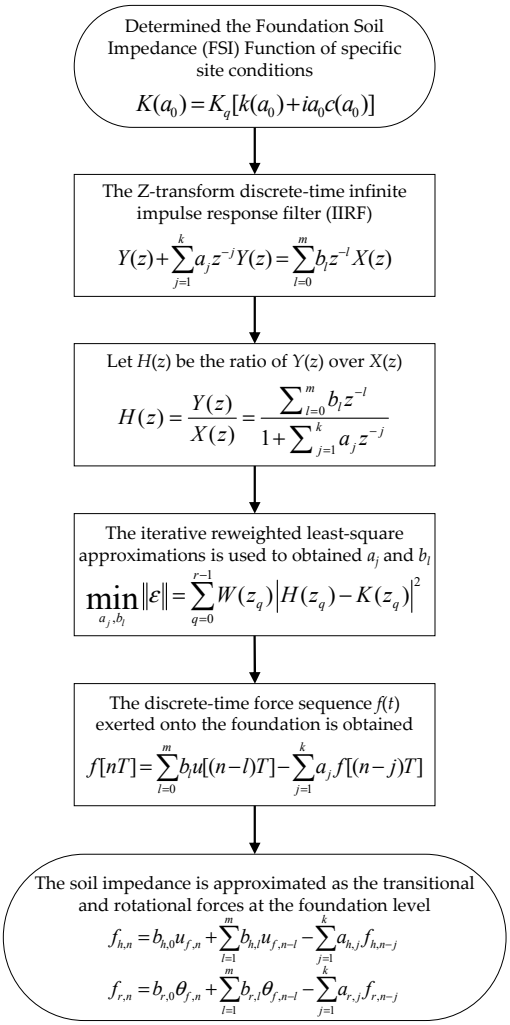

Figure 2. Flowchart depicting the process of determining the translational and rotational forces through the use of the IIRF technique.

2.2. Motion Equations Considering SSI Effects and Superstructure's Inelasticity

Equation (1) is used to formulate the equation of motion for the 3DOF SSI-based SFS system at a specific time instance n.

$$\begin{bmatrix} m_s & 0 & 0 \\ 0 & m_f & 0 \\ 0 & 0 & I_f \end{bmatrix} \begin{Bmatrix} \ddot{u}_{s,n} \\ \ddot{u}_{f,n} \\ \ddot{\theta}_{f,n} \end{Bmatrix} + \begin{bmatrix} c_s & -c_s & -c_s h \\ -c_s & c_s & c_s h \\ -c_s h & c_s h & c_s h^2 \end{bmatrix} \begin{Bmatrix} \dot{u}_{s,n} \\ \dot{u}_{f,n} \\ \dot{\theta}_{f,n} \end{Bmatrix} + \begin{bmatrix} k_s & -k_s & -k_s h \\ -k_s & k_s & k_s h \\ -k_s h & k_s h & k_s h^2 \end{bmatrix} \begin{Bmatrix} u_{s,n} \\ u_{f,n} \\ \theta_{f,n} \end{Bmatrix} + \begin{Bmatrix} 0 \\ f_{h,n} \\ f_{r,n} \end{Bmatrix} = - \begin{Bmatrix} m_s \\ m_f \\ 0 \end{Bmatrix} \ddot{u}_{g,n} \quad (1)$$

where

m_s = mass of the superstructure
m_f = mass of the foundation
I_f = moment inertia of the foundation
c_s = damping of the superstructure
k_s = stiffness of the superstructure

The terms u_s, u_f, θ_f and $\dot{u}_s$, $\dot{u}_f$, $\dot{\theta}_f$ and $\ddot{u}_s$, $\ddot{u}_f$, $\ddot{\theta}_f$ denote the displacement or rotational angle and their first- and second-order derivatives, and $\ddot{u}_g$ is the ground acceleration. The subscripts s and f represent structure- and foundation-related, respectively.

Equation (1) is intentionally restructured into the format of Equation (2) by relocating the terms $\overline{f}_{h,n}$ and $\overline{f}_{r,n}$ to the right-hand side of the equation. The terms $\overline{f}_{h,n}$ and $\overline{f}_{r,n}$, as the partial contents of the horizontal force $f_{h,n}$ and moment $f_{r,n}$, respectively, can be derived from the known quantities $u_{f,n-1}$, $\theta_{f,n-1}$, $f_{h,n-1}$ and $f_{r,n-1}$ of the previous time step. Such practice can avoid recalculation of $\overline{f}_{h,n}$ and $\overline{f}_{r,n}$ during the time-wise iteration, thereby enhancing the efficiency of the overall calculation process.

$$\begin{bmatrix} m_s & 0 & 0 \\ 0 & m_f & 0 \\ 0 & 0 & I_f \end{bmatrix} \begin{Bmatrix} \ddot{u}_{s,n} \\ \ddot{u}_{f,n} \\ \ddot{\theta}_{f,n} \end{Bmatrix} + \begin{bmatrix} c_s & -c_s & -c_s h \\ -c_s & c_s & c_s h \\ -c_s h & c_s h & c_s h^2 \end{bmatrix} \begin{Bmatrix} \dot{u}_{s,n} \\ \dot{u}_{f,n} \\ \dot{\theta}_{f,n} \end{Bmatrix} + \begin{bmatrix} k_s & -k_s & -k_s h \\ -k_s & k_s + b_{h,0} & k_s h \\ -k_s h & k_s h & k_s h^2 + b_{r,0} \end{bmatrix} \begin{Bmatrix} u_{s,n} \\ u_{f,n} \\ \theta_{f,n} \end{Bmatrix} = -\begin{Bmatrix} m_s \\ m_f \\ 0 \end{Bmatrix} \ddot{u}_{g,n} + \begin{Bmatrix} 0 \\ \overline{f}_{h,n} \\ \overline{f}_{r,n} \end{Bmatrix} \quad (2)$$

$$\overline{f}_{h,n} = -\sum_{j=1}^{p} b_{h,j} u_{f,n-j} + \sum_{i=1}^{k} a_{h,i} f_{h,n-i} \quad (3)$$

$$\overline{f}_{r,n} = -\sum_{j=1}^{p} b_{r,j} \theta_{f,n-j} + \sum_{i=1}^{k} a_{r,i} f_{r,n-i} \quad (4)$$

Literally, Equation (2) represents the motion equation obtained under the assumption of a linear system. However, to account for the nonlinear behavior of the superstructure, the Takeda hysteresis model illustrated in Figure 3 was utilized to depict the force-displacement relationship of the superstructure during cyclic elastic–plastic evolution. The superstructure's stiffness k_s in Equation (2) is no longer a constant but a variable that changes with the deformation process associated with loading, unloading, and reloading. Figure 3 demonstrates that this study defines several stiffness components, including the initial stiffness k_0, the post-yielding stiffness factor r, and power law constant α.

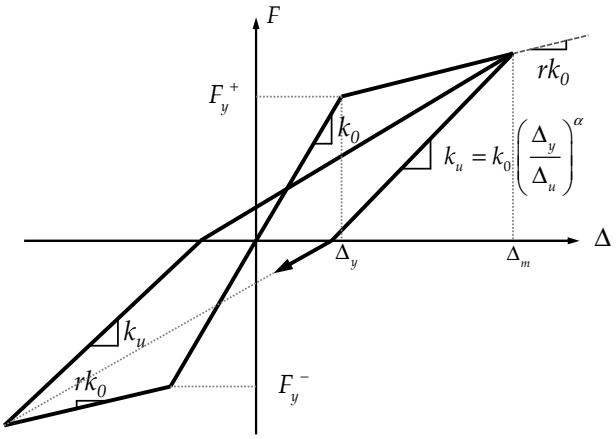

Figure 3. Takeda's hysteretic model.

2.3. Formulation of Energy Equations

To derive the mechanical energy quantities of the defined SSI-based SFS system during a ground motion excitation, Equation (1) is reorganized into the following three equilibrium equations for a particular time instant t:

$$m_s\ddot{u}_s(t) + c_s\dot{u}_s(t) - c_s\dot{u}_f(t) - c_sh\dot{\theta}_f(t) + k_su_s(t) - k_su_f(t) - k_sh\theta_f(t) = -m_s\ddot{u}_g(t) \quad (5)$$

$$m_f\ddot{u}_f(t) - c_s\dot{u}_s(t) + c_s\dot{u}_f(t) + c_sh\dot{\theta}_f(t) - k_su_s(t) + k_su_f(t) + k_sh\theta_f(t) + f_h = -m_f\ddot{u}_g(t) \quad (6)$$

$$I_f\ddot{\theta}_f(t) - c_sh\dot{u}_s(t) + c_sh\dot{u}_f(t) + c_sh^2\dot{\theta}_f(t) - k_shu_s(t) + k_shu_f(t) + k_sh^2\theta_f(t) + f_r = 0 \quad (7)$$

Through integration of Equations (5)–(7) w.r.t. $u_s(t)$, $u_f(t)$, and $\theta_f(t)$, respectively, the energy equation for each degree of freedom is obtained:

$$\begin{array}{c}\int m_s\ddot{u}_s(t)du_s + \int c_s\dot{u}_s(t)du_s - \int c_s\dot{u}_f(t)du_s - \int c_sh\dot{\theta}_f(t)du_s \\ +\int k_su_s(t)du_s - \int k_su_f(t)du_s - \int k_sh\theta_f(t)du_s = -\int m_s\ddot{u}_g(t)du_s\end{array} \quad (8)$$

$$\begin{array}{c}\int m_f\ddot{u}_f(t)du_f - \int c_s\dot{u}_s(t)du_f + \int c_s\dot{u}_f(t)du_f + \int c_sh\dot{\theta}_f(t)du_f \\ -\int k_su_s(t)du_f + \int k_su_f(t)du_f + \int k_sh\theta_f(t)du_f + \int f_hdu_f = -\int m_f\ddot{u}_g(t)du_f\end{array} \quad (9)$$

$$\begin{array}{c}\int I_f\ddot{\theta}_f(t)d\theta_f - \int c_sh\dot{u}_s(t)d\theta_f + \int c_sh\dot{u}_f(t)d\theta_f + \int c_sh^2\dot{\theta}_f(t)d\theta_f \\ -\int k_shu_s(t)d\theta_f + \int k_shu_f(t)d\theta_f + \int k_sh^2\theta_f(t)d\theta_f + \int f_rd\theta_f = 0\end{array} \quad (10)$$

From the view of energy dissipation mechanism, the above energy quantities can be classified into kinetic energy, $E_k(t)$, damping energy, $E_d(t)$, recoverable strain energy, $E_s(t)$, yielding energy, $E_Y(t)$, SSI-related energy, $E_{SSI\text{-}related}(t)$, and input energy, $E_{in}(t)$, as defined in Equations (11)–(15).

The kinetic energy is associated with the work undertaken by the inertial forces in the components of the system. The recoverable strain energy and yielding energy are dependent on the structural stiffness. The seismic input energy is primarily dissipated through the hysteresis damping of the superstructure and the SSI effect caused by supporting soil, which is alternatively represented through the work undertaken by the transitional and rotational foundation forces in this study.

$$E_k(t) = \int_0^{u_s} m_s\ddot{u}_s(t)du_s + \int_0^{u_f} m_f\ddot{u}_f(t)du_f + \int_0^{\theta_f} I_f\ddot{\theta}_f(t)d\theta_f \quad (11)$$

$$\begin{array}{c}E_d(t) = \int_0^{u_s} c_s\dot{u}_s(t)du_s - \int_0^{u_s} c_s\dot{u}_f(t)du_s - \int_0^{u_s} c_sh\dot{\theta}_f(t)du_s \\ -\int_0^{u_f} c_s\dot{u}_s(t)du_f + \int_0^{u_f} c_s\dot{u}_f(t)du_f + \int_0^{u_f} c_sh\dot{\theta}_f(t)du_f \\ -\int_0^{\theta_f} c_sh\dot{u}_s(t)d\theta_f + \int_0^{\theta_f} c_sh\dot{u}_f(t)d\theta_f + \int_0^{\theta_f} c_sh^2\dot{\theta}_f(t)d\theta_f\end{array} \quad (12)$$

$$\begin{array}{c}E_Y(t) + E_s(t) = \int_0^{u} k_su_s(t)du_s - \int_0^{u} k_su_f(t)du_s - \int_0^{u} k_sh\theta_f(t)du_s \\ -\int_0^{u_f} k_su_s(t)du_f + \int_0^{u_f} k_su_f(t)du_f + \int_0^{u_f} k_sh\theta_f(t)du_f \\ -\int_0^{\theta_f} k_shu_s(t)d\theta_f + \int_0^{\theta_f} k_shu_f(t)d\theta_f + \int_0^{\theta_f} k_sh^2\theta_f(t)d\theta_f\end{array} \quad (13)$$

$$E_{SSI-related}(t) = \int_0^{u_f} f_h(t)du_f + \int_0^{\theta_f} f_r(t)d\theta_f \quad (14)$$

$$E_{in}(t) = -\int_0^{u_s} m_s\ddot{u}_g(t)du_s - \int_0^{u_f} m_f\ddot{u}_g(t)du_f \quad (15)$$

Based on the energy conservation theorem, the energy equilibrium equation can be written as

$$E_{in}(t) = E_k(t) + E_d(t) + E_s(t) + E_Y(t) + E_{SSI-related}(t) \quad (16)$$

2.4. Determination of SSI-Related Damping Ratio

This study used a work–energy theorem equation to determine the SSI-related Damping Ratio (SSIDR), as presented in Equation (17). The SSI-related energy dissipated is equalized with the energy dissipated by an equivalent viscous system during one vibration cycle:

$$E_{SSIDR}(t) = \int f_{SSI-related}du = \int_0^{2\pi/\omega} (c_{SSI-related}\dot{u})\dot{u}dt = \int_0^{2\pi/\omega} c_{SSI-related}\dot{u}^2dt = 2\pi\xi_{SSI-related}\frac{\omega}{\omega_n}ku_0^2 \quad (17)$$

where

ω = circular frequency of excitation
ω_n = natural circular frequency of the system
u_0 = maximum displacement of the structure in one cycle

$\xi_{SSI\text{-}related}$ = SSI-related Damping Ratio (SSIDR)
$c_{SSI\text{-}related}$ = SSI-related damping coefficient in one loading cycle $= 2k\xi_{SSI-related}/\omega_n$

In the paper, the frequency-related impedance function is presented in the time domain through the aforementioned IIRF system, and the energy equation expressed by applying the SSIDR is defined in Equation (18). The energy entity E_{SSIDR} signifies the energy dissipated due to SSI effect during a period of [0, t].

$$E_{SSIDR}(t) = \int_0^t f_{SSI-related}\dot{u}dt = \int_0^t c_{SSI-related}\dot{u}^2dt = \frac{2\xi_{SSI-related}k}{\omega_n}\int_0^t \dot{u}^2dt \quad (18)$$

Meanwhile, the energy dissipated by the inherent damping of the superstructure can be expressed as

$$E_d(t) = \int_0^t c\dot{u}^2dt = \frac{2\xi_0 k}{\omega_n}\int_0^t \dot{u}^2dt \quad (19)$$

where ξ_0 denotes the inherent damping ratio of the superstructure. Accordingly, the SSIDR can then be defined as

$$\xi_{SSI-related}(t) = \xi_0\frac{E_{SSIDR}}{E_d} = \xi_0\frac{\int_0^t f_d\dot{u}dt}{\int_0^t c\dot{u}^2dt} \quad (20)$$

When under an earthquake excitation, the $\xi_{SSI\text{-}related}$ value varies as the time elapses. To circumvent the needs for determining the energy quantities and $\xi_{SSI\text{-}related}$ at discrete time instants, this study calculated the $\xi_{SSI\text{-}related}$ in the form of the total system energy.

3. Implementation Study

A procedure of using the energy method to evaluate the SSI-related damping in a bridge pier system was developed based on the methods and techniques elaborated in Section 2. This section presents a bridge pier case to demonstrate an implementation procedure.

Theoretically, the proposed SSI-based SFS system is developed by expanding an SDOF model to include the SSI effects (e.g., damping) via the IIRF technique. As the base stone, the accuracy of the fixed-base SDOF model is of great importance.

Therefore, the case study is conducted by first referencing a previous experimental bridge pier study to verify the feasibility of the fixed-base SDOF model, and then conducting seismic analyses on the IIRF-integrated SFS system to explore the SSI effects on the relative displacement responses. Furthermore, great emphasis was laid on the energy dissipation mechanism of the SSI-based SFS system and the role of SSI-related energy dissipating in a quantitative manner (i.e., SSIDR) when different earthquake recordings were considered.

3.1. Experimental Study of Bridge Pier

To illustrate the proposed method and provide a comparison object, an experimental study by Chang et al. [29] was referenced. Chang et al. conducted a series of experimental studies on the hysteresis performance of bridge columns under particular ground excitations. The experimental studies involved three identical reinforced-concrete (RC) bridge piers (Specimens A–C), which were designed according to the 1995 Taiwan Bridge Design Code, and the geometry and reinforcement details of the as-built specimens are illustrated in Figure 4. The loading conditions were designed so that Specimen A was subjected to a cyclic loading at the specimen's bottom, and that Specimens B and C were during real earthquake recordings. The masses of 27,500 kg and 68,000 kg were applied via a load cell to Specimens B and C, respectively.

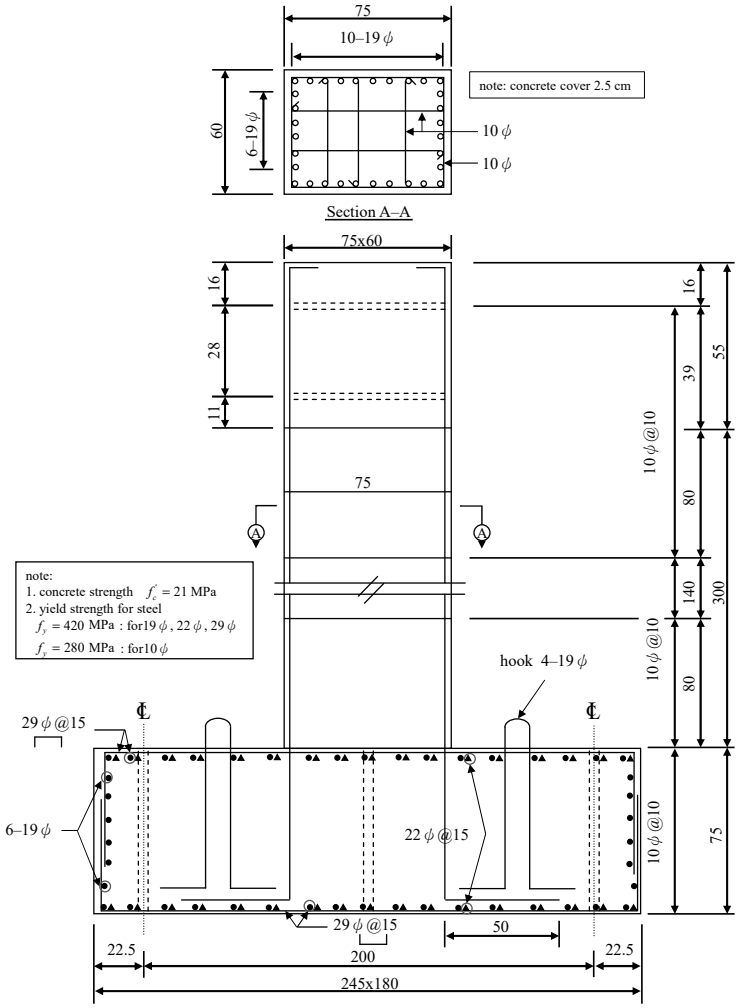

Figure 4. Geometry and reinforcement details of the bridge pier specimens.

In Chang et al.'s study, the loading conditions of Specimens B and C adopted the ground motion data recorded during the 1999 Chi-Chi Earthquake, Taiwan, at the stations of TCU075 and TCU102. Figures 5 and 6 separately display the 30-s ground acceleration and velocity time-histories of the earthquake TCU075 recording with the PGA = 0.8 g and TCU102 recording with the PGA = 0.7 g.

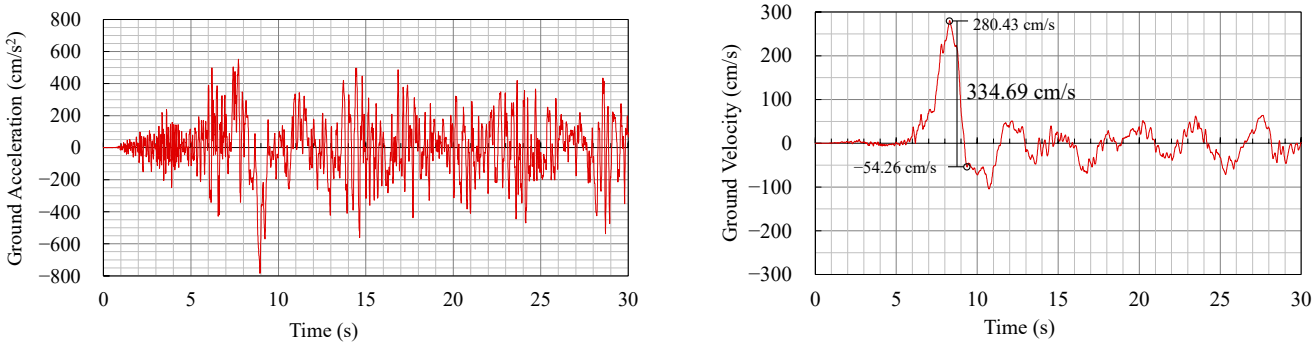

Figure 5. Ground motion time-histories of Station TCU075: (**a**) acceleration and (**b**) velocity time-history.

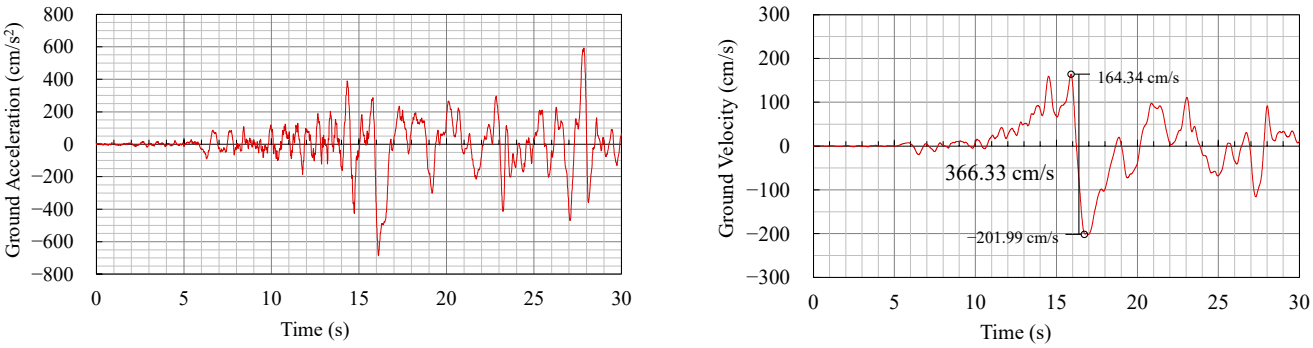

(**a**) (**b**)

Figure 6. Ground motion time-histories of Station TCU102: (**a**) acceleration and (**b**) velocity time-history.

It is noted that both ground excitation records exhibit pulse-like velocity patterns. For example, in the TCU075 ground motion, the ground velocity spikes from nearly zero to its maximum of 280.43 cm/s within a short time duration and then transits to 54.26 cm/s in the opposite direction, and the maximum incremental velocity (MIV) is 334.69 cm/s (+280.43 → −54.26 cm/s). However, TCU102 exhibits a rather opposite fashion in that the velocity instantaneously transits from the upper side peak of 164.34 cm/s to the bottom side peak of 201.99 cm/s, while the MIV is 366.33 cm/s (+164.34 → −201.99 cm/s).

The variance between the TCU075 and TCU102 recordings lay in the fact that the ground velocity from the upper side peak had a large intensity and the bottom side peak had a moderate intensity in the TCU075 recording, i.e., large-to-moderate MIV, and, by contrast, in the TCU102 recording, the ground velocity from the upper side peak had a large intensity to the bottom side peak with a large intensity, i.e., large-to-large MIV.

3.2. Verification of Bridge Pier Fixed-Base SDOF System

According to the results of Specimen A subjected to the cyclic loading, the lateral yielding force F_y = 411.68 kN with the yielding displacement Δy = 42.23 mm, and the ultimate force F_u = 432.69 kN with the ultimate displacement Δu = 150 mm. Based on the results, a Takeda's model (Figure 3) can be formulated with k_0 = 9748.78 MPa, r = 0.06, and a = 0.5 to present the bridge pier specimens' elastic–plastic behavior. For the dynamic characteristics of Specimens B and C, the elastic structural period is 0.3337 s and 0.5248 s, respectively.

The fundamental dynamic characteristic of the test can be modeled by an SDOF system using lumped mass and experimental stiffness. A MATLAB-compiled simple fixed-base SDOF bridge pier model that incorporated the derived Takeda's model was constructed, with the superstructure's damping ratio of 5%. Dynamic simulations were then conducted by subjecting the inelastic fixed-base SDOF pier model to the earthquake TCU075 and TCU102 recordings (Figures 5 and 6).

The resultant restoring force and mass-to-foundation relative displacement are displayed in Figures 7 and 8, and the corresponding results of Chang et al.'s study are also depicted for a comparison purpose. According to the results during the earthquake TCU075 recording (large-to-moderate MIV), the maximum lateral restoring force and displacement in the experiment study were 466.97 kN and 68.32 mm, occurring at t = 14.52 s (Figure 7), in contrast to the analytical counterpart of 426.86 kN and 68.18 mm.

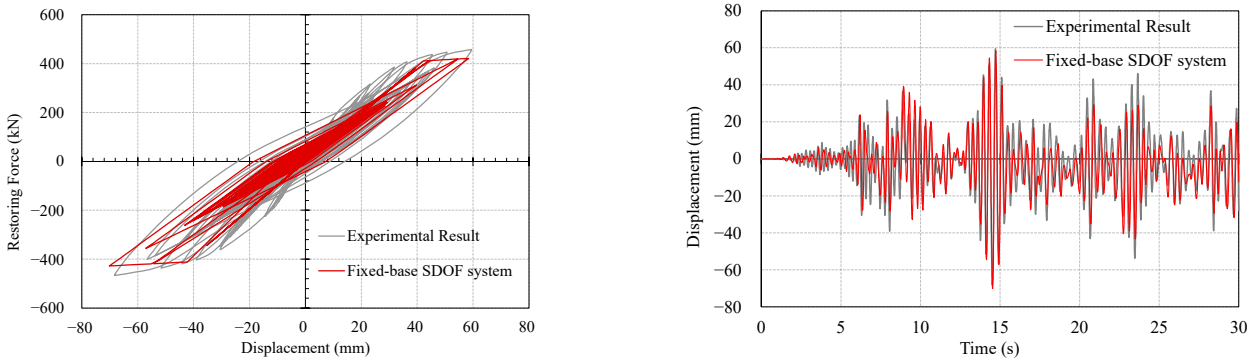

(**a**) (**b**)

Figure 7. Comparison between analytical and experimental results subjected to ground motion recording of Station TCU075: (**a**) hysteretic loops and (**b**) displacement time-history.

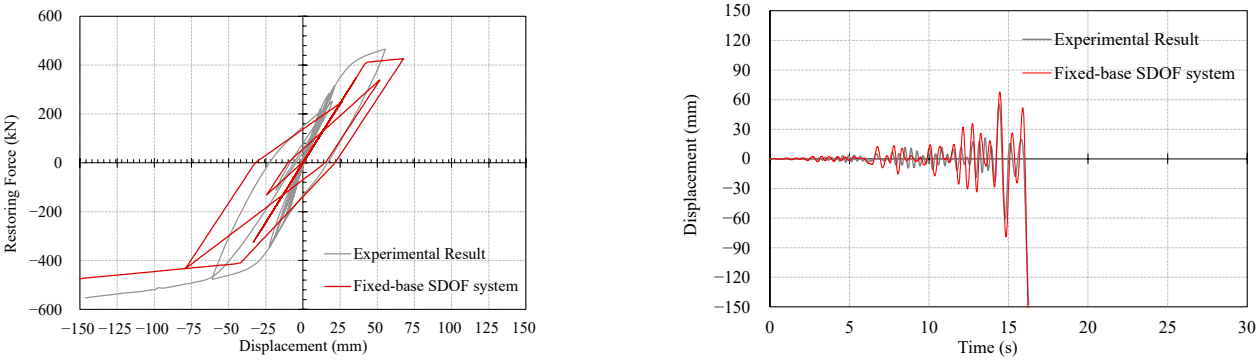

(**a**) (**b**)

Figure 8. Comparison between analytical and experimental results subjected to ground motion recording of Station TCU102: (**a**) hysteretic loops and (**b**) displacement time-history.

Likewise, for the earthquake TCU102 recording (large-to-large MIV), the maximum lateral restoring force and displacement in the experiment were 476.78 kN and 60.98 mm at t = 14.79 s, while the analytical responses, simultaneously, were 429.08 kN and 72.66 mm (Figure 8). Because pronounced concrete cover spalling and reinforcement buckling occurred at the bottom of the specimen during the test, the test was halted at t = 16.27 s to avoid unpredictable catastrophes.

Given the resemblance of the hysteresis loops and displacement time-history, as well as the consistency of the maximum lateral restoring force and displacement, it is sensible to deduce that the inelastic fixed-base SDOF bridge pier model is reliable for later use as the foundation for developing the IIRF-integrated SSI-based SFS system.

3.3. Dynamic Analyses of Bridge Pier SFS System

By applying the methods stated in Sections 2.1 and 2.2, the verified inelastic fixed-base SDOF bridge pier model was expanded to include the SSI effect via the discrete-time IIRF technique to develop the target SFS system. Figure 9 and Table 1 exhibit the modeling parameters for the soil and the foundation.

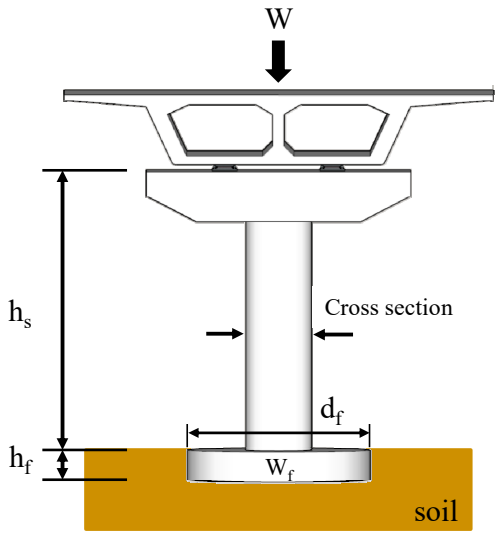

Figure 9. Geometry details of the bridge pier specimens.

Table 1. Modeling Parameters of the Superstructure, Foundation, and Soil.

Superstructure	
Superstructure Height h_s (m)	3.55
Superstructure Cross Section (m)	0.75 × 0.6
Superstructure Stiffness (MPa)	9748.78
Superstructure's Damping Ratio	0.05
Post-yielding Stiffness Factor r	0.06
Power Law Constant α	0.5
Foundation	
Foundation Height h_f (m)	0.9
Foundation Mass W_f (kg)	27,143
Foundation Diameter d_f (m)	4
Soil	
Shear Modulus G (kN/m^2)	29,964
Shear Wave Velocity V_s (m/s)	365
Poisson's Ratio v	1/3

This study employed soil conditions with the shear wave velocity V_S = 365 m/s. The superstructure of the SSI-based SFS model was assumed to be supported by a rigid disk foundation and an underlying uniform-soil half-space. The rigid disk foundation is 0.9 m in height and 4 m in diameter, with a mass of 27,143 kg.

Figures 10 and 11 and Table 2 present the analytical results of the SSI-based SFS simulation during the earthquake TCU075 or TCU102 recordings, in contrast to those of the corresponding fixed-base SDOF simulation.

Table 2. Range of the mass-to-foundation relative displacement (mm) of the SSI-based SFS and Fixed-base SDOF systems during the earthquake TCU075 and TCU102 recordings.

Earthquake Recording	SSI-Based SFS System	Fixed-Base SDOF System
TCU075	+57.84~−72.04	+58.23~−70.14
TCU102	+104.5~−89.13	+67.63~−79.01

Note: the positive and negative signs denote the fore- and aft-movement directions, respectively.

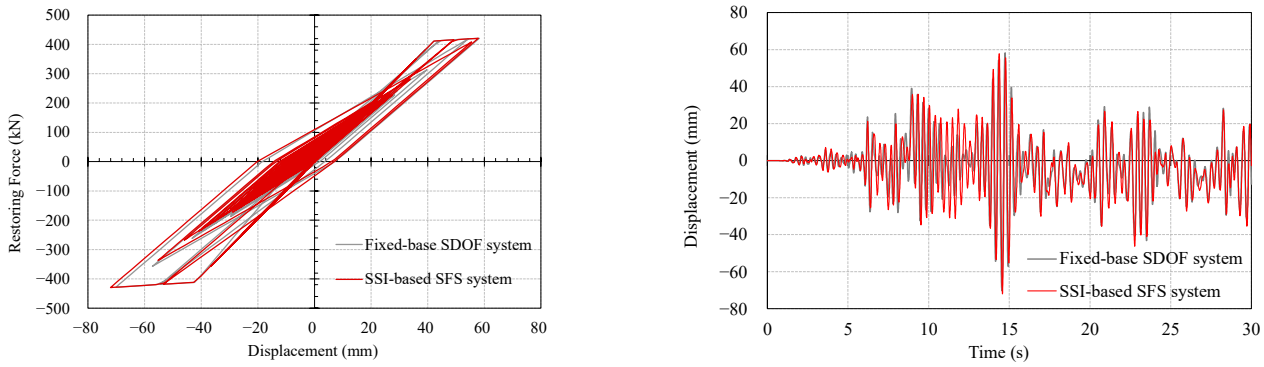

(**a**) (**b**)

Figure 10. Analytical result comparison between SSI-based SFS and Fixed-base SDOF systems during ground motion recording of Station TCU075: (**a**) hysteretic loops and (**b**) displacement time-history.

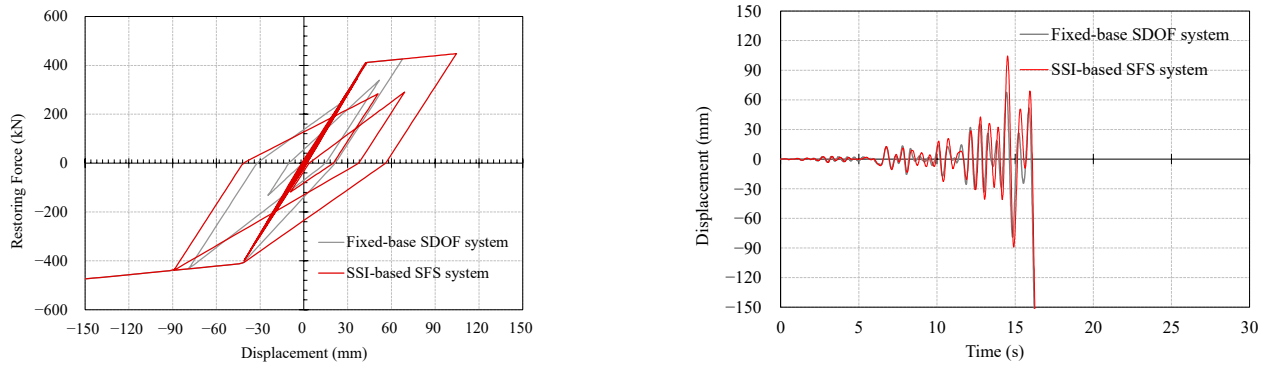

(**a**) (**b**)

Figure 11. Analytical result comparison between SSI-based SFS and Fixed-base SDOF systems during ground motion recording of Station TCU102: (**a**) hysteretic loops and (**b**) displacement time-history.

From the above results, it was found that:

1. As to the earthquake TCU075 recording (large-to-moderate MIV), when the SSI effect was considered, the hysteresis loops and the mass-to-foundation relative displacement time-history displayed good resemblance between the SSI-based SFS and fixed-base SDOF systems.
2. As to the earthquake TCU102 recording (large-to-large MIV), the SSI-based SFS system exhibited wider hysteresis loops and larger superstructure displacement responses than the fixed-base SDOF system. This indicated an amplification effect of the soil on the earthquake excitation and the corresponding superstructure responses.

In this study, frequency domain analysis was conducted on the structural system responses of the Fixed-base SDOF System and SSI-based SFS System using Fourier transform. The influence of the SSI effect on the structural period was investigated during different near-fault ground motions. Figures 12 and 13 show the Fourier spectra of the Fixed-base SDOF System and SSI-based SFS System, respectively, for the earthquake recordings TCU075 and TCU102. The structural periods are summarized in Table 3. Compared with the elastic period, the structural periods are larger as the structure enters the inelastic phase. Additionally, the results show that considering SSI can prolong the structural period (from 0.390 s to 0.410 s) during the earthquake TCU075 recording (large-to-moderate MIV). Meanwhile, during the earthquake TCU102 recording (large-to-large MIV), there is no difference in the Fourier transform of structural responses between the SFS System and Fixed-base SDOF System (0.640 s). This indicates that the SSI effect is suppressed during the earthquake TCU102 recording (large-to-large MIV).

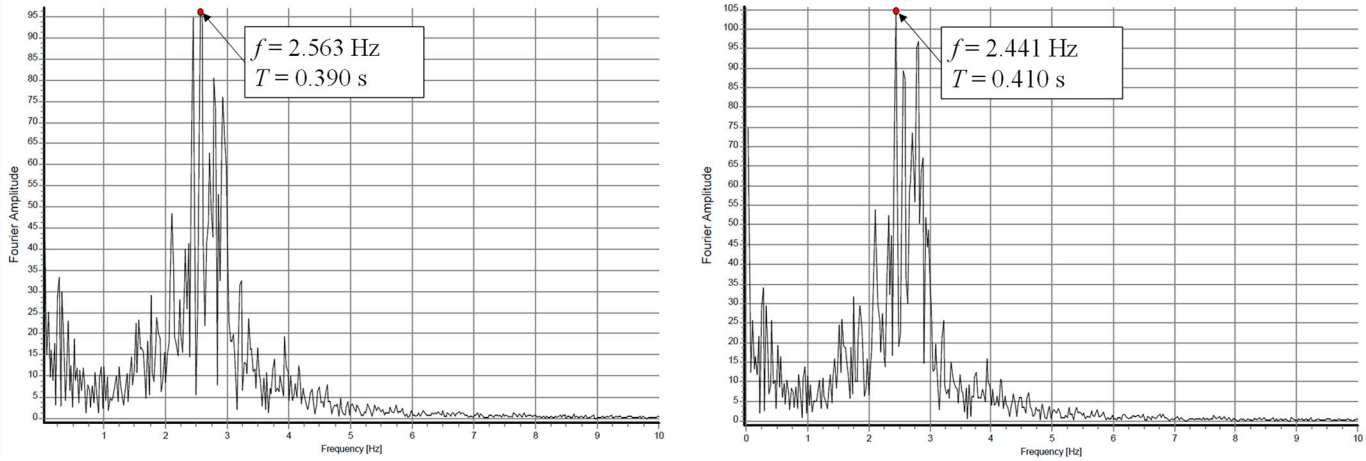

(**a**) (**b**)

Figure 12. Fourier transform analytical results during ground motion recording of Station TCU075: (**a**) Fixed-base SDOF system and (**b**) SSI-based SFS system.

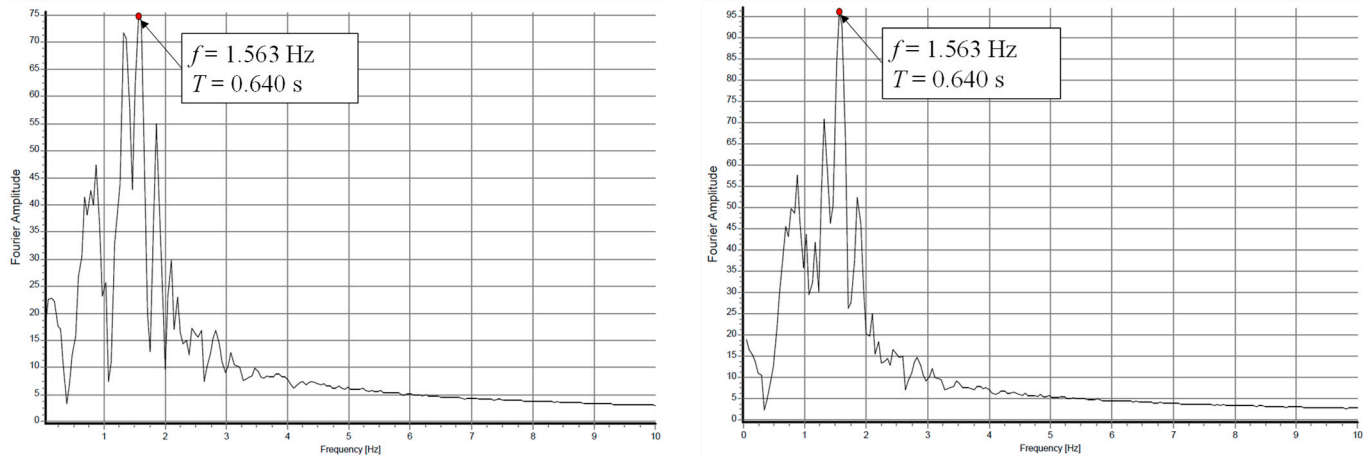

(**a**) (**b**)

Figure 13. Fourier transform analytical results during ground motion recording of Station TCU102: (**a**) Fixed-base SDOF system and (**b**) SSI-based SFS system.

Table 3. The structural period of the SSI-based SFS and Fixed-base SDOF systems during the earthquake TCU075 and TCU102 recordings.

Earthquake Recording	Fixed-Base SDOF System	SSI-Based SFS System
TCU075	0.390 s	0.410 s
TCU102	0.640 s	0.640 s

The above observation exhibits the SSI effects on the displacement response of the superstructure in a qualitative manner, not rending an overview performance of the superstructure, foundation, and soil as a whole. The next section attempts, from an energy viewpoint, to discuss the SSI-based SFS system energy dissipation mechanism and the role of soil in energy dissipation in a quantitative manner.

3.4. Energy Time-History Analysis Considering SSI Effect

According to the formulation of energy equation mentioned in Section 2.4 and the above analytical results of the SSI-based SFS system subjected to two near-fault earthquake recordings, this study obtained the separate energy quantities of damping energy, E_d,

recoverable strain energy, E_s, yielding energy, E_Y, SSI-related energy, $E_{SSI\text{-}related}$, and input energy, E_{in}, as defined in Equations (12)–(15) and shown in Figures 14 and 15.

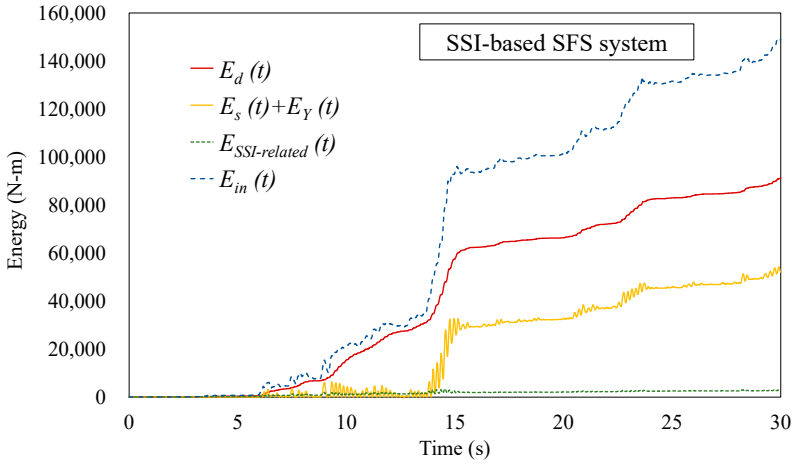

Figure 14. Energy time-histories of the SSI-based SFS system during ground motion recording of Station TCU075.

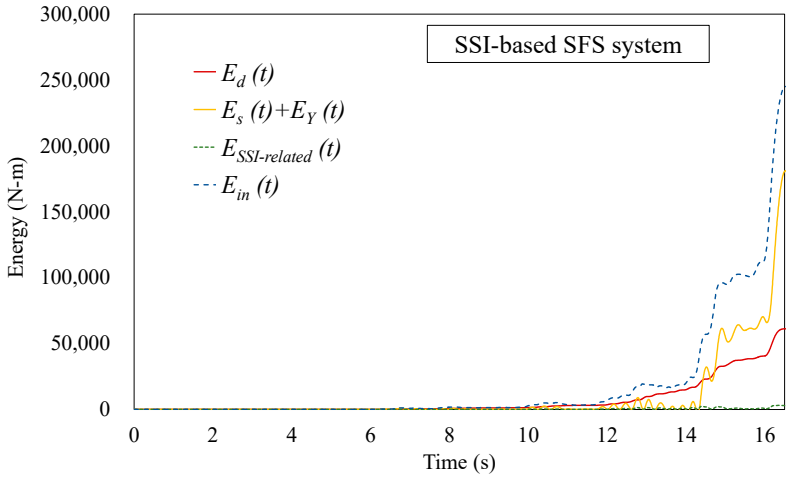

Figure 15. Energy time-histories of the SSI-based SFS system during ground motion recording of Station TCU102.

It can be seen from Figure 14 that as the time elapses from the initiation of the earthquake TCU075 recording (large-to-moderate MIV), the input energy E_{in} gradually increases till a considerable leap occurs at t = 14–15 s. Such leaping fashion simultaneously happens to the energy sum of recoverable strain energy E_s and yielding energy E_Y; this indicates that the superstructure enters its inelastic domain concurrently. Notably, the maximum velocity pulse (Figure 5b) does not coincide with the energy leaping.

Likewise, Figure 15 gives the energy time history of the SSI-based SFS system during the earthquake TCU102 recording (large-to-large MIV). The maximum velocity pulse occurred at approximately t = 16 s (Figure 6b), followed by an excitation cease considering the prevention of possible structural catastrophe, as shown in Figure 8b. In other words, the original earthquake TCU102 recording was modified by truncating the excitation trace at t = 16.27 s, after which the ground motion ceased.

In the TCU102 earthquake recording case, no pronounced SSI-related energy dissipation appears (Figure 15). Such variance may be attributable to the fact that the two earthquake recordings have distinct ground motion traces. As shown in Figure 6b, TCU102 exhibits a fashion that the velocity instantaneously transits from one side peak to the other side peak, with a velocity change of 366.33 cm/s. Such sudden large-to-large MIV may

cause the soil to not be able to react in a short time and the structure suddenly reaches its failure limit.

Table 4 presents the energy quantities integrated over time regarding the earthquake recordings, and the percentage of the total input energy is determined and presented in Table 4.

Table 4. Summary of Energy Quantities in the SSI-based SFS Systems.

Earthquake Recording	Energy Quantities of the SSI-Based SFS System (kN-m-s) (The Values in the Parentheses Signify the Percentage of the Total Input Energy)			
	E_k	E_d	$E_s + E_Y$	$E_{SSI\text{-}related}$
TCU075	30.240 (1.51%)	1293.964 (64.797%)	624.996 (31.297%)	47.764 (2.392%)
TCU102	29.956 (9.091%)	121.821 (36.970%)	172.764 (52.431%)	4.969 (1.508%)

According to Table 4, conclusions can be drawn as follows:

1. During the earthquake TCU075 recording (large-to-moderate MIV), the SSI-related energy $E_{SSI\text{-}related}$ took up only 2.4% of the total earthquake energy, whereas the damping energy E_d and the strain and yielding energy $E_s + E_Y$ accounted for 64.8% and 31.3%, respectively.
2. During the earthquake TCU102 recording (large-to-large MIV), the velocity pulse shifted too fast to initiate the SSI-related energy dissipation action; therefore, the SSI-related energy percentage was rather small, i.e., $E_{SSI\text{-}related}$ = 1.51% E_{in}. Given the fact that the strain and yielding energy $E_s + E_Y$ = 52.34%, it is sensible to deduce that the superstructure undertook the majority of energy by exerting its inelastic performance, with minor SSI effects on energy consumption.

3.5. SSIDR Determination

Through the IIRF method, the frequency-dependent characteristics of the soil can be transformed into the time domain for dynamic analysis. As a result, the SSI effect (including the dynamic stiffness and damping property of the soil) were approximated as the transitional force and rotational moment at the foundation level. Therefore, the work done by the transitional force and rotational moment can be regarded as the SSI-related energy of the SSI-based SFS system.

According to the characteristics of cumulated damping and recoverable strain energy, the SSI-related energy illustrated in Figure 16 can be disassembled into the recoverable strain energy and cumulated damping energy.

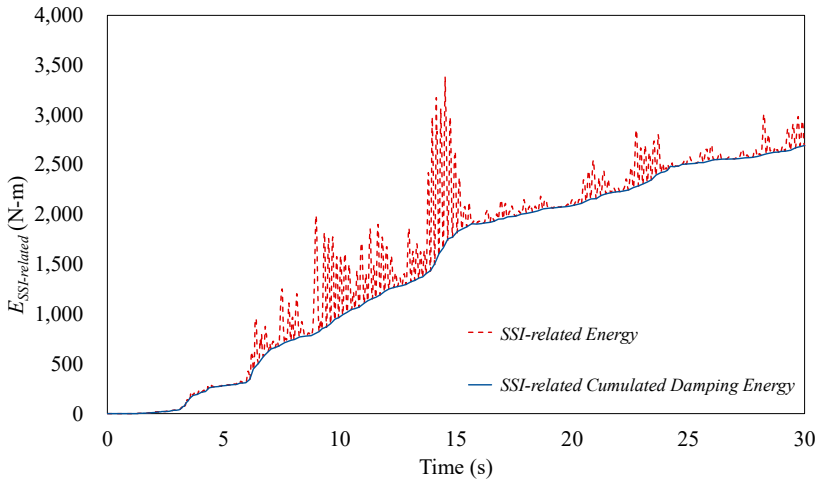

Figure 16. SSI-related energy time-history of the SSI-based SFS system.

Because the SSIDR is a variable during the time-history process, this study used the total system energy to calculate the representative SSIDR during a specific earthquake. The resultant SSIDRs are presented in Table 5, and a solid trend can be found: The small SSIDR values during the earthquake TCU102 recording (large-to-large MIV) indicated minor SSI effects on the system, and that the majority of the earthquake energy was dissipated through the inelastic performance of the superstructure. This observation is consistent with the findings in Section 3.3, where the SFS system's structural period was not prolonged due to the SSI effect during the earthquake TCU102 recording (large-to-large MIV), indicating that the SSI effects are suppressed during near-fault earthquakes with large-to-large MIV characteristics.

Table 5. Summary of the SSIDR in the SSI-based SFS system.

Earthquake Recording	SSIDR (%)
TCU075 (large-to-moderate velocity transition)	0.167
TCU102 (large-to-large velocity transition)	0.066

4. Conclusions

This study proposed a procedure of using the energy method to evaluate the SSI-related damping effects on the responses of bridge pier structures. Through the IIRF method, the frequency-dependent SSI function was transferred into the time domain to formulate the motion equation of the bridge pier SSI-based SFS inelastic system. Based on the motion equation, the energy dissipation mechanism was formulated to explore the SSI-related and superstructure energy distribution separately. Taketa's model, with the model parameters calibrated experimentally, was used to account for the elastic–plastic behavior of the bridge pier system. Therefore, the energy consumed by the superstructure yielding can be quantitatively determined. Finally, the SSIDR was obtained from the intrinsic damping ratio and the ratio of the SSI-related energy to the superstructure damping energy. Instead of achieving the SSIDR at each instant, this study determined an overall SSIDR based on the total system energy scale.

Furthermore, an implementation study was conducted based on a previous experimental study to compare the response variance between distinct input earthquake recordings, and the primary findings are briefly summarized as follows:

1. Earthquakes with large-to-large MIV may lead to low SSIDRs. For those with large-to-large MIV features, considering the decrease in the SSI effect, the structure may be exerted towards more nonlinear behaviors.
2. Regardless of the earthquake TCU075 or TCU102 recording, the SSI effect was suppressed when the SFS system underwent near-fault earthquakes. This phenomenon illustrated that the stiffness and damping contribution from the soil was not pronounced.

Author Contributions: Conceptualization, K.-H.C.; methodology, K.-H.C.; software, K.-H.C.; supervision, Y.-C.S. and C.-K.S.; validation, X.-Q.L. and C.-K.S.; visualization, Y.-C.S.; writing—original draft, K.-H.C.; writing—review and editing, X.-Q.L. All authors have read and agreed to the published version of the manuscript.

Funding: This research was supported by the Ministry of Science and Technology in Taiwan. (Project No.: 109-2221-E-027-003-MY3).

Data Availability Statement: Data will be made available on request.

Conflicts of Interest: The authors declare that they have no known competing financial interests or personal relationships that could have appeared to influence the work reported in this paper.

References

1. Chopra, A.K.; Gutierrez, J.A. Earthquake response analysis of multistorey buildings including foundation interaction. *Earthq. Eng. Struct. Dyn.* **1974**, *3*, 65–77. [CrossRef]
2. Novak, M. Effect of soil on structural response to wind and earthquake. *Earthq. Eng. Struct. Dyn.* **1974**, *3*, 79–96. [CrossRef]
3. Veletsos, A.S.; Meek, J.W. Dynamic behavior of building-foundation systems. *Earthq. Eng. Struct. Dyn.* **1974**, *3*, 121–138. [CrossRef]
4. Wang, J.; Guo, T.; Du, Z. Experimental and numerical study on the influence of dynamic structure-soil-structure interaction on the responses of two adjacent idealized structural systems. *J. Build. Eng.* **2022**, *52*, 104454. [CrossRef]
5. Zhang, X.; Far, H. Effects of dynamic soil-structure interaction on seismic behaviour of high-rise buildings. *Bull. Earthq. Eng.* **2022**, *20*, 3443–3467. [CrossRef]
6. Carbonari, S.; Dezi, F.; Padrón, L.A.; Zimmaro, P. Preface to special issue on modelling and assessment of soil-structure interaction effects on the dynamics of structures. *Bull. Earthq. Eng.* **2022**, *20*, 3071–3076. [CrossRef]
7. Bielak, J. Dynamic response of non-linear building-foundation systems. *Earthq. Eng. Struct. Dyn.* **1978**, *6*, 17–30. [CrossRef]
8. Rodriguez, M.E.; Montes, R. Seismic response and damage analysis of buildings supported on flexible soils. *Earthq. Eng. Struct. Dyn.* **2000**, *29*, 647–665. [CrossRef]
9. Avilés, J.; Pérez-Rocha, L.E. Soil–structure interaction in yielding systems. *Earthq. Eng. Struct. Dyn.* **2003**, *32*, 1749–1771. [CrossRef]
10. Hassani, N.; Bararnia, M.; Amiri, G.G. Effect of soil-structure interaction on inelastic displacement ratios of degrading structures. *Soil. Dyn. Earthq. Eng.* **2018**, *104*, 75–87. [CrossRef]
11. Cao, X.Y.; Feng, D.C.; Beer, M. Consistent seismic hazard and fragility analysis considering combined capacity-demand uncertainties via probability density evolution method. *Struct. Saf.* **2023**, *103*, 102330. [CrossRef]
12. Anand, V.; Kumar, S.S. Sensitivity of strength reduction factor for structures considering soil-structure interaction. *Structures* **2022**, *39*, 593–606. [CrossRef]
13. Avcı, Y.; Yazgan, U. Probabilistic estimation of inelastic displacement demands in soil–structure interaction systems on cohesive soils. *Earthq. Eng. Struct. Dyn.* **2022**, *51*, 22–43. [CrossRef]
14. Gazetas, G. Analysis of machine foundation vibrations: State of the art. *Soil Dyn. Earthq. Eng.* **1983**, *2*, 2–42. [CrossRef]
15. Luco, J.E. Impedance functions for a rigid foundation on a layered medium. *Nucl. Eng. Des.* **1974**, *31*, 204–217. [CrossRef]
16. Veletsos, A.S.; Wei, Y. Lateral and rocking vibration of footings. *J. Soil Mech. Found. Div.* **1971**, *97*, 1227–1248. [CrossRef]
17. Apsel, R.J.; Luco, J.E. Impedance functions for foundations embedded in a layered medium: An integral equation approach. *Earthq. Eng. Struct. Dyn.* **1987**, *15*, 213–231. [CrossRef]
18. Şafak, E. Time-domain representation of frequency-dependent foundation impedance functions. *Soil Dyn. Earthq. Eng.* **2006**, *26*, 65–70. [CrossRef]
19. Gash, R.; Seylabi, E.E.; Taciroglu, E. Implementation and stability analysis of discrete-time filters for approximating frequency-dependent impedance functions in the time domain. *Soil. Dyn. Earthq. Eng.* **2017**, *94*, 223–233. [CrossRef]
20. Sung, Y.C.; Chen, C.C. Z-Transferred discrete-time infinite impulse response filter as foundation–soil impedance function for SDOF dynamic structural response considering soil–structure interaction. *Earthq. Spectra* **2019**, *35*, 1003–1022. [CrossRef]
21. *ATC-32*; Improved Seismic Design Criteria for California Bridges: Provisional Recommendation. Applied Technology Council: Redwood City, CA, USA, 1996.
22. *ASCE-7-16*; Minimum Design Loads and Associated Criteria for Buildings and Other Structures. American Society of Civil Engineers: Reston, VA, USA, 2017.
23. Veletsos, A.S. Dynamics of structure-foundation systems. In *Structural and Geotechnical Mechanic*; Hall, W.J., Ed.; Prentice-Hall: Englewood Cliffs, NJ, USA, 1977; pp. 333–361.
24. Sieffert, J.G.; Cevaer, F. *Handbook of Impedance Function: Surface Foundations*; Ouest Editions Presses Academiques: Nantes, France, 1991.
25. McKevitt, W.E.; Anderson, D.L.; Cherry, S. Hysteretic energy spectra in seismic design. In Proceedings of the 2nd World Conference on Earthquake Engineering, Tokyo and Kyoto, Japan, 11–18 July 1960; Volume 7, pp. 487–494.
26. Uang, C.M.; Bertero, V.V. Evaluation of seismic energy in structures. *Earthq. Eng. Struct. Dyn.* **1990**, *19*, 77–90. [CrossRef]
27. Bruneau, M.; Wang, N. Some aspects of energy methods for the inelastic seismic response of ductile SDOF structures. *Eng. Struct.* **1996**, *18*, 1–12. [CrossRef]
28. Hu, X.; Chen, Q.; Weng, D.; Zhang, R.; Ren, X. Estimation of additional equivalent damping ratio of the damped structure based on energy dissipation. *Adv. Civ. Eng.* **2019**, *2019*, 8052413. [CrossRef]
29. Chang, S.Y.; Li, Y.F.; Loh, C.H. Experimental study of seismic behaviors of as-built and carbon fiber reinforced plastics repaired reinforced concrete bridge columns. *J. Bridge Eng.* **2004**, *9*, 391–402. [CrossRef]